ACS APPLIED MATERIALS & INTERFACES

Research Article

www.acsami.org

Multiscale Analysis of Changes in an Anisotropic Collagen Gel Structure by Culturing Osteoblasts

Yohei Hanazaki,[†] Jyun-ichi Masumoto,[†] Shoichi Sato,[†] Kazuya Furusawa,[‡] Akimasa Fukui,[‡] and Naoki Sasaki*[,‡]

[†]Transdisciplinary Life Science Course, Graduate School of Life Science, Hokkaido University, Kita-10, Nishi-8, Kita-ku, Sapporo, Japan

[‡]Faculty of Advanced Life Science, Hokkaido University, Kita-10, Nishi-8, Kita-ku, Sapporo, Japan

Supporting Information

ABSTRACT: Mimicking the complicated anisotropic structures of a native tissue is extremely important in tissue engineering. In a previous study, we developed an anisotropic collagen gel scaffold (ACGS) having a hierarchical structure and a properties gradient. In this study, our objective was to see how cells remodel the scaffolds through the cells−ACGS interaction. For this purpose, we cultured osteoblastic cells on ACGS, which we regarded as a model system for the cells−extracellular matrix (cell-ECM) interaction. Changes in the ACGS−cell composites structure by cell-ECM interactions was investigated from a macroscopic level to a microscopic level. Osteoblastic cells were also cultured on an isotropic collagen gel (ICGS) as a control. During the cultivation, mechanical stimuli were applied to collagen-cell composites for adequate matrix remodeling. Confocal laser scanning microscope (CLSM) was used to observe macroscopic changes in the ACGS−cell composite structure by osteoblastic cells. Small-angle X-ray scattering (SAXS) measurements were performed to characterize microscopic structural changes in the composites. Macroscopic observations using CLSM revealed that osteoblastic cells remained only in the diluted phase in ACGS and they collected collagen fibrils or formed a toroidal structure, depending on the depth from the ACGS surface in the tubular diluted phase. The cells were uniformly distributed in ICGS. SAXS analysis suggests that collagen fibrils were remodeled by osteoblastic cells, and this remodeling process would be affected by the structure difference between ACGS and ICGS. These results suggest that we directly regulate cell-ECM interaction by the unique anisotropic and hierarchical structure of ACGS. The cell−gel composite presented in this study would promise an efficient scaffold material in tissue engineering.

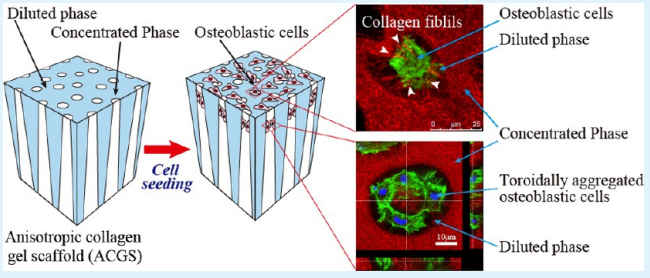

KEYWORDS: *anisotropic collagen gel, hierarchical structure, property gradient, osteoblast, small angle X-ray scattering, matrix remodeling*

1. INTRODUCTION

The most important property required for scaffolds in tissue engineering is their ability to completely mimic native tissue structures, as tissue structure affects cell activities such as cell morphology, proliferation, and differentiation through cell−extracellular matrix (cell-ECM) interactions.[1,2] In this context, various types of scaffolds have been developed so far. However, a scaffold with almost the same structure as that of native tissue has not been produced, because mimicking the complicated anisotropic structures of native tissues has been a source of great difficulty.

Furthermore, native tissue has properties that gradually change in space, resulting in a properties gradient, such as a stiffness gradient.[3] Biomaterials helping a tissue generation often have a properties or structural gradient.[4] It is expected that such a properties gradient, derived from inhomogeneous structures of native tissue, could help cells to perform remodeling of the tissue through cell-ECM interactions.

To mimic anisotropic structure of native tissue, anisotropic collagen scaffolds have been developed for tissue engineering so far.[5−10] For example, Lanfer et al. fabricated anisotropic collagen scaffold using flow deposition technique for osteoblast cultivation, and succeeded to osteoblast alignment along to the collagen orientation.[5] Lai et al. developed anisotropic collagen scaffold that consisted of macroscopically aligned collagen strings using a straightforward flow processing technique.[6] Isobe et al. and Mikami et al. fabricated various three-dimensional (3D) anisotropic collagen scaffolds, such as mesh sheet or tube with the flow processing method, and conducted successful in vivo transplant experiments.[7,8]

From a therapeutic point of view, these scaffolds are very useful. However, collagen scaffolds that have a hierarchical

Received: October 25, 2012
Accepted: June 11, 2013
Published: June 11, 2013

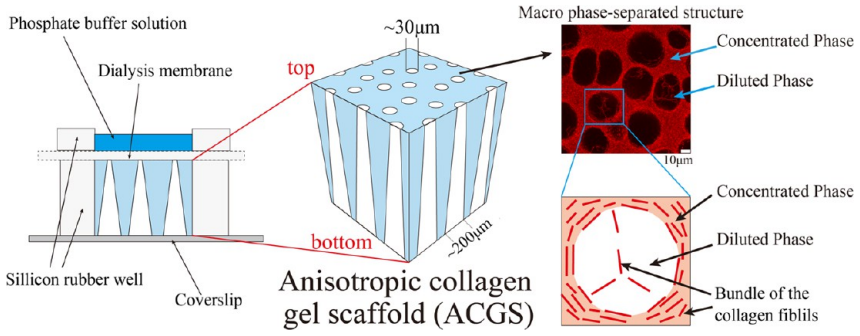

Figure 1. Schematic diagram of anisotropic collagen gel scaffold (ACGS). ACGS is prepared from collagen solution and phosphate buffer solution (PBS). The gel has a phase-separated structure. It has a high collagen concentration region (concentrated phase) and a low collagen concentration region (diluted phase). Diameter of the diluted phase is gradually changed ~30−200 μm from top to bottom of the gel. Magnified schematic image of ACGS at the diluted phase shows that collagen fibrils were oriented circumferentially to the interface and diluted phase is not empty space but a small number of bundles of the collagen fibrils exists.[10] Scale bar = 10 μm.

structure from the molecular level to the tissue level and a properties gradient due to inhomogeneity have not been fabricated. The anisotropic scaffold that has both hierarchical structure and property gradient is useful for investigating cell-ECM interactions and can lead to developing a novel scaffold for tissue engineering.

In our previous work, we prepared an anisotropic collagen gel by dialysis of collagen solutions into phosphate buffer solution with neutral pH values.[11,12] We confirmed that the anisotropic collagen gel (ACGS) had a hierarchical structure and a properties gradient.[11,12] Generally, the interaction of cells with their matrix has been known to change with the change in matrix properties. When cells are cultured on a matrix having a properties gradient, the interaction would be highlighted. Since ACGS has a properties gradient, such an observation of a cells-ECM interaction is expected. The study on the interaction is necessary for understanding the effect of the scaffold when used for therapeutic purposes. The objective of the present study was to see how cells remodel the scaffolds as the result of a cell-ECM interaction through the cultivation of cells on ACGS. For this purpose, we cultured osteoblastic cells on ACGS, which we regarded as a model system for the cell-ECM interaction. Changes in the ACGS−cell composites structure by remodeling was investigated from a macroscopic level to microscopic level. The cultured cell-gel composite was investigated macroscopically by confocal laser scanning microscopy and microscopically by small-angle X-ray scattering (SAXS). The results were discussed how cells adopt ACGSs based on the morphology observation.

The structure of the ACGS is shown in Figure 1. The gel has a phase-separated structure. It has a high collagen concentration region (concentrated phase) and a low collagen concentration region (diluted phase), and showed birefringence (see Figure 1 in the Supporting Information). The diameter of the diluted phase is gradually changed by ~30−200 μm from top to bottom of the gel, and such a structure is related to a property gradient. A magnified schematic picture of ACGS (see inset of Figure 1 in the Supporting Information) shows that collagen fibrils were oriented circumferentially to the interface and small number of the bundle of the collagen fibrils is existed in the diluted phase. ACGS is different from isotropic collagen gel scaffolds that were prepared by a traditional method (ICGSs) at the point that ACGS has an anisotropic, hierarchy structure from a molecular level to a macroscopic gel level and has a properties gradient. ICGS did not show birefringence, as observed in ACGS (see Figure 1 in the Supporting Information).

We used the osteoblastic MC3T3-E1 cell line as the testing cells, because they are one of the most studied cells. Residing in bone tissue, osteoblasts are responsible for bone mineralization by the secretion of calcium phosphates and for the remodeling of bone. In the latter process, osteoblasts secrete collagenase to digest collagen and reconstruct a collagen matrix.[13] Mechanical stimuli (MS) have long been regarded to play an important role in osteoblast differentiation.[14−16] In previous research, pre-osteoblastic cells were cultured in bone-mimic matrices to investigate the effect of MS on osteoblastic differentiation.[17−25] Therefore, we applied MS to the ACGS−osteoblast composite.

MATERIALS AND METHODS

1. Solution Preparation. We used an "atelo-collagen" for this study, which was purchased in 5 mg/mL 1 mM HCl aqueous solution at pH 3.0 from Koken Co., Ltd. (Tokyo, Japan). A phosphate buffer solution (PBS) consisting of KH_2PO_4 and Na_2HPO_4 (Wako Pure Chemical Co., Ltd., Osaka, Japan) was prepared. Concentrations of KH_2PO_4 and Na_2HPO_4 were 13 mM and 20 mM, respectively. The pH of PBS was 7.0 at 30 °C.

The growth medium was Minimum Essential Medium Alpha (MEMα, Wako) supplemented with 10% FBS (fetal bovine serum; PAA Laboratories, Austria) and 1% penicillin−streptomycin (Sigma Chemicals, St. Louis, MO, USA). The differential medium was the growth medium supplemented with 2 mM glycerophosphate disodium salt pentahydrate (MP Biomedicals, Irvine, CA, USA) and 50 μg/mL L-ascorbic acid phosphate magnesium salt *n*-hydrate (Wako).

2. ACGS and ICGS Preparation. Figure 2 shows the schematic illustration of a dialysis chamber (10 mm in diameter, 3 mm in thicknesses) to prepare collagen gel scaffolds. The collagen solution chamber consists of two silicon rubber sheets with a thickness of 1.5 mm set on a 35-mm cell culture plastic dish (Thermo Scientific, Waltham, MA, USA). The collagen solution (150 μL) was injected into the chamber. A dialysis membrane was set on the top of the collagen solution chamber, and a silicon rubber well was then put on the dialysis membrane. To prepare ACGS, PBS was poured over the silicon rubber well. Conversely, the growth medium was poured over the silicon rubber well to prepare ICGS. During the dialysis process of the collagen solution into PBS or the growth medium, the collagen gel phase grew from the dialysis membrane from the top to the bottom of the chamber. Scaffolds were incubated for 2 h at 30 °C. After removing PBS and the dialysis membrane, scaffolds were immersed in the growth medium and incubated overnight in a 37 °C, 5% CO_2 incubator. For application of MS, the upper silicon rubber sheet was removed before cell seeding on scaffolds. To observe the macroscopic morphology of ACGS and ICGS, we took optical images using a DMC-GF2 digital camera (Panasonic Corporation, Osaka, Japan) and

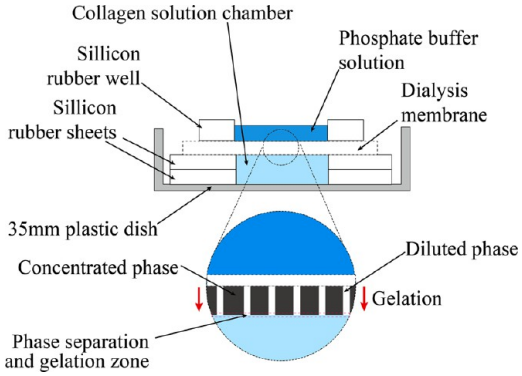

Figure 2. Scheme of anisotropic and isotropic gel formation. The collagen solution chamber consisted of two 1.5-mm-thick silicon rubber sheets and is placed on a 35-mm plastic dish. Both silicon rubbers have a 10-mm-diameter circular hole. A total of 200 μL of collagen solution were injected into the chamber. A dialysis membrane was set on the top of the collagen solution chamber, and then the silicon rubber well was put on the dialysis membrane. PBS was poured over the silicon rubber well to make ACGS. Growth medium was poured over the silicon rubber well to make ICGS. During the dialysis process of the collagen solution against PBS or the growth medium, the collagen gel phase grew from the dialysis membrane from the top to the bottom of the collagen solution chamber.

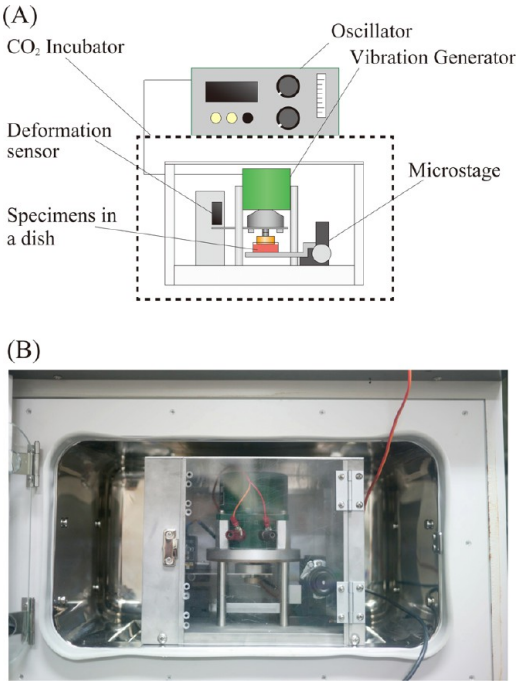

Figure 3. (A) Scheme and (B) a picture of the MS application apparatus. The device was placed in the 37 °C, 5% CO_2 incubator. The deformation sensor monitors the deformation of a specimen in real time. The oscillator and vibration generator make a sinusoidally vibrating movement of the aluminum indenter. The aluminum indenter is disk-shaped, 10 mm in thickness and 30 mm in diameter. The specimen was set on the stage. A periodic compressive strain was directly applied to specimens, using the aluminum indenter.

NANOHA x5 ultramacro lenses (Yasuhara Co. Ltd., Nagoya, Japan) under natural light, polarized light, and circular polarized light (see Figure 1 in the Supporting Information).

3. Cell Culture. The osteoblastic cell line (MC3T3-E1 cells) was provided by RIKEN BRC through the National Bio-Resource Project of MEXT, Japan. MC3T3-E1 cells were cultured in the growth medium. Cells were cultured on a cell culture plastic dish (FG-2090; Nippon Genetics Co., Ltd., Tokyo, Japan) in an incubator regulated at 37 °C and 5% CO_2. Cells at passage 5 were seeded on ACGS (MC3T3-E1/ACGS composite) and ICGS (MC3T3-E1/ICGS composite). Seeding density was 3.0×10^4 cells/gel. Two days after seeding, the medium was changed to the differentiation medium. The medium was changed every 3 days. Specimens were taken from a dish at day 7, day 14, and day 21, and these were used in the following experiments.

4. MS Application. MS was applied to MC3T3-E1 cells using the MS-application apparatus shown in Figure 3. The device monitors compressive deformation by a deformation sensor in real time. The device was placed in the 37 °C, 5% CO_2 incubator. The specimen was set on the stage. A cyclic compressive strain was directly applied to specimens by an aluminum indenter (10 mm in thickness, 30 mm in diameter, cylindrical shape). Strain amplitude and the frequency of MS were controlled at 3000 $\mu\varepsilon$ and 3 Hz, respectively (see Figure 2 in the Supporting Information). MS was applied for 1 h per day from day 0 to day 6.

5. Conforcal Laser Scanning Microscope Observation. To observe the morphology of specimens, collagen molecules, actin fibers, and nuclei were visualized using immunofluorescence staining for collagen molecules, Alexa Fluor 488-conjugated phalloidin (Molecular Probes, Life technologies Corporation, CA, USA) for actin fibers, and SYTOX Blue (Molecular Probes) for nuclei, respectively.

A blocking solution, primary antibody solution, and a secondary antibody solution were prepared. The blocking solution consisted of 10% FBS and 0.5% Triton X-100 (Wako) in phosphate buffer saline consisting of 2.3 mM of KCl, 1.5 mM of KH_2PO_4, 8.4 mM of Na_2HPO_4, and 137 mM of NaCl at pH 7.4 (PBS(−)). An anticollagen alpha I (SC-8784-R, Santa Cruz Biotechnology, Inc., CA, USA) diluted 1:200 in the blocking solution was used as the primary antibody solution. An Alexa Fluor 633-conjugated antirabbit IgG (Molecular Probes, Life Technologies Corporation, CA, USA) diluted 1:1000 in the blocking solution was used as the secondary antibody solution. 300 units of Alexa Fluor 488-conjugated phalloidin solution was diluted 1:60 in PBS(−). 5 mM of SYTOX Blue solution was diluted 1:5000 in PBS(−).

5.1. Collagen Staining. Specimens were washed with PBS(−) three times, then fixed by 4% formaldehyde for 30 min at 4 °C. Specimens were blocked and permeabilized with blocking solution at room temperature for 3 h. Specimens were then incubated with the primary antibody solution overnight at room temperature. Specimens were washed three times with PBS(−), followed by incubation at room temperature for 3 h in the secondary antibody solution.

5.2. Actin Fiber Staining. Specimens were washed three times with PBS(−) and were then treated with phalloidin solution for 3 h.

5.3. Cell Nucleus Staining. Specimens were stained with SYTOX Blue solution for 1 h. Specimens were mounted on a coverslip and observed via confocal laser scanning microscopy (CLSM) (Leica, Model TCS SP5).

We took a surface region image (from the gel surface to a depth of 30 μm) and an inner region image (30−60 μm deep) for each specimen. We counted cell numbers in a 450 μm × 450 μm area at each region.

6. SAXS Measurements. SAXS measurements were performed at the BL40B2 beamline equipped in the SPring-8 (Japan Synchrotron Radiation Research Institute; JASRI). The X-ray wavelength was 1.5 Å. The incident X-ray beam was parallel to the growth direction of the collagen gel layer (Figure 3 in the Supporting Information). The sample-to-detector distance was 4250 mm. SAXS patterns were acquired with a CCD camera (Model C4880, Hamamatsu Photonics, Shizuoka, Japan) with an X-ray imaging intensifier (Model IV4554P, Hamamatsu Photonics). Exposure times were 5 s or 10 s. We selected the proper exposure time for each specimen to prevent a saturating scattering intensity. All experiments were performed at 37 °C. Two-dimensional (2D) SAXS patterns were corrected by subtracting the dark current of the detector. To obtain one-dimensional (1D) SAXS profiles, the circular average of 2D SAXS patterns were calculated. The

averaged scattering intensity $I(q)$ was plotted as a function of scattering vector q, defined as

$$q = \frac{4\pi}{\lambda} \sin\left(\frac{2\theta}{2}\right)$$

where 2θ is the scattering angle.

7. Statistical Analysis. All experiments were performed three times. Statistical differences were assessed using a one-way analysis of variance (ANOVA). Calculations were performed by SigmaPlot (version 11.0, Hulinks, Inc., Tokyo, Japan).

RESULTS AND DISCUSSION

1. Confocal Laser Scanning Microscope Observation. Low-magnification CLSM images of MC3T3-E1 cells/ACGS (anisotropic gel) composites (ACGS-MS$^-$), MC3T3-E1 cells/ICGS (isotropic gel) composites (ICGS-MS$^-$), mechanically stimulated MC3T3-E1 cells/ACGS composites (ACGS-MS$^+$), and mechanically stimulated MC3T3-E1 cells/ICGS composites (ICGS-MS$^+$) at 14 days cultivation are shown in Figures 4A, 4B, 4C, and 4D, respectively. The cells existed uniformly and densely in surface regions. Significant differences in cell distribution on the surface region were not observed among all specimens. This result suggests that ACGS has as good a cell attachment and biocompatibility as ICGS. In the inner region of ACGS, osteoblastic cells were found only in the diluted phase (see Figures 4A and 4B). In contrast, the cells were observed individually and randomly in the inner region of ICGS (see Figures 4C and 4D). These results suggest that osteoblastic cells invading into collagen gels may recognize elasticity distribution in the matrix. In ICGS, where the elasticity of the matrix is uniform, the cells would distribute homogeneously and randomly, while in ACGS, the elasticity of the matrix is different in the diluted phase and concentrated phase, and the interface between the two phases has the highest difference in elasticity. As reported in the literature, osteoblasts prefer migrating on the stiffer matrix.[26−28] In ACGS, collagen molecular density in the concentrated phase (ρ_C) is larger than those of ICGS (ρ_{ICGS}). The density of the diluted phase in ACGS ρ_D is smaller than that of ICGS ($\rho_C > \rho_{ICGS} > \rho_D$). This means the order of modulus in each phase should be $E_C > E_{ICGS} > E_D$ (the subscripts C, ICGS, and D have the same meaning as those in ρ). Cells in ICGS might migrate by developing the space through protease digestion. The permeation of cells would be the easiest in the diluted phase of ACGS. Therefore, osteoblastic cells would migrate into ACGS by attaching onto the interfacial walls between dilute and concentrated phases in ACGS.

The magnified image of the shallow and deep parts of ACGS-MS$^-$ specimen at 14 days of cultivation is shown in Figures 4E and 4F, respectively. In the shallow part of the diluted phase of ACGS, osteoblastic cells seemed to pull and collect collagen fibrils from the concentrated phase (see Figure 4E). This result suggests that collagen fibrils in the diluted phase of ACGS would be modified by the cells. In the deep region of ACGS, where the diameter of the diluted phase increased, the cells constructed a toroidal structure along with the wall of the diluted phase, and relatively concentrated collagen fibrils were observed in the center of the diluted phase (see Figure 4F). These results indicate that osteoblastic cells attach onto the interface between the diluted and concentrated phases and that they increase the concentration of collagen fibrils at the center of the diluted phase. With the change in diameter of the diluted phase, the morphology of the cell in the diluted phase changed.

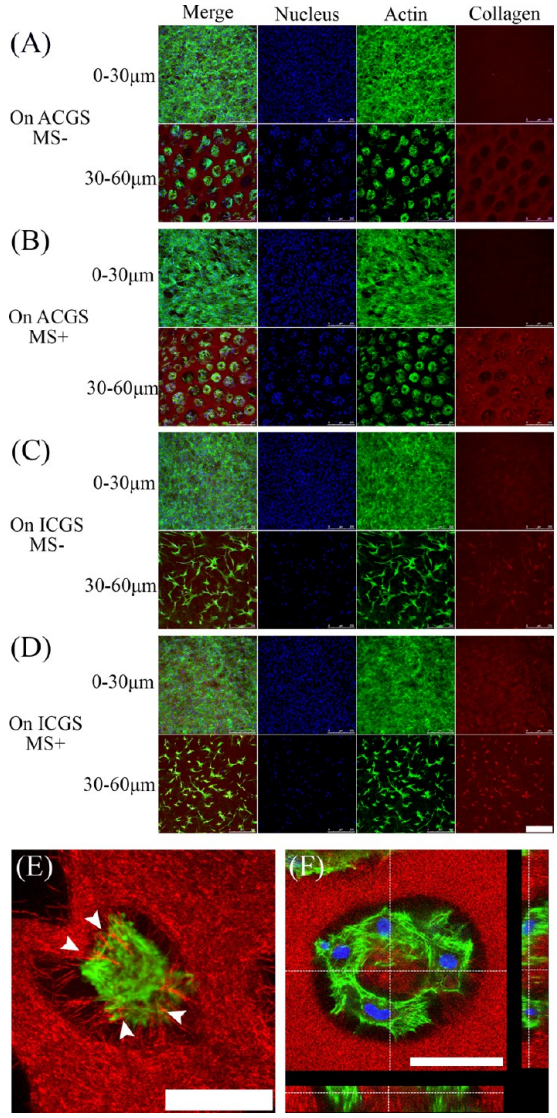

Figure 4. CLSM images of the cell−gel composites. (A−D) Low-magnification CLSM images of surface or inner region of each specimen ((A) ACGS-MS, (B) ACGS-MS$^+$, (C)ICGS-MS$^-$, and (D) ICGS-MS$^+$, each at 14 days of cultivation). The surface region is 0−30 μm, and 30−60 μm is the inner region of each specimen. Scale bar = 250 μm. (E) Z-stack magnified image of osteoblastic cells in the diluted phase of ACGS-MS$^-$ at 7 days of cultivation. Red represents collagen, and green represents actin fibers. The cells appeared to be pulling collagen fibers from the interfacial wall between concentrated and diluted phases into the diluted phase of ACGS (arrow heads). Scale bar = 25 μm. (F) Z-stack magnified image of osteoblastic cells in the diluted phase of ACGS-MS$^-$ at 14 days of cultivation. Red represents collagen, Blue represents nuclei, and green represents actin fibers. The cells form a toroidal aggregation structure in the diluted phase, and they collected collagen fibers in the center of the diluted phase. Scale bar = 25 μm.

Altogether, cell−matrix interaction and cell morphology varied along with the variation in anisotropic structure of ACGS.

A schematic diagram of osteoblastic cell invasion into ACGS is shown in Figure 5. At first, the cells proliferated on the ACGS surface to become confluent. Then, they started to invade into the inner region (Figure 5A). Osteoblastic cells collected the collagen fibrils in the diluted phase at the shallow region (Figure 5B). However, in the deep region, as the diameter of the dilute phase increased, the cells would attach on the

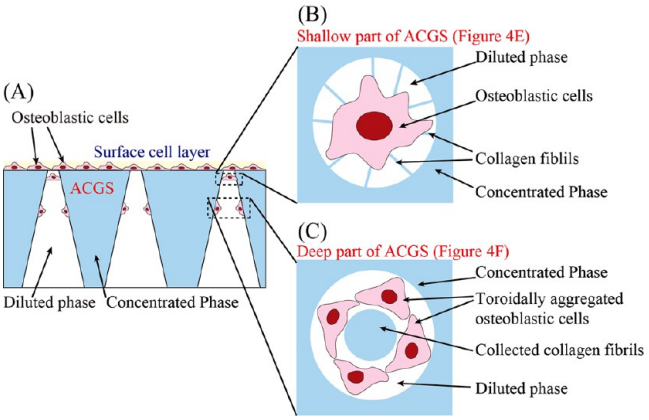

Figure 5. Schematic diagram of an ACGS−cell composite. (A) Cross-sectional view of the ACGS−cell composite; at the ACGS surface, osteoblastic cells form a cell layer, and some cells invaded into the diluted phase. (B) Schematic diagram of Figure 4E; the cells exist in the diluted phase, and they appear to be pulling a bundle of the collagen fibrils from the interfacial wall between concentrated and diluted phases. (C) Schematic diagram of Figure 4F; the cells attach onto the interface to construct a toroidally aggregating structure. Collagen fibrils that were presumably collected by the cells existed in the center of the diluted phase.

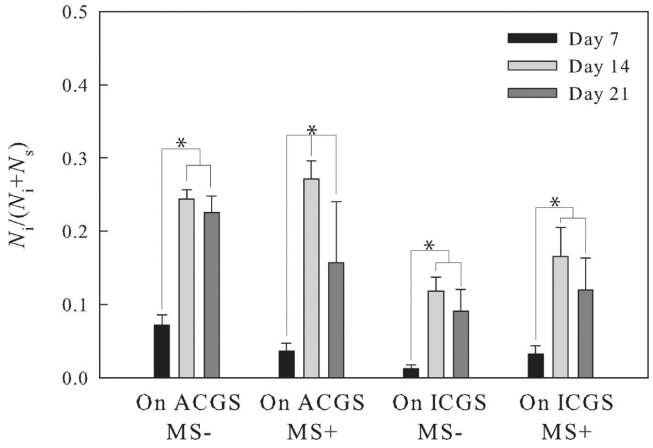

Figure 6. Quantification of cell numbers, along with the time course of cell culture (from 7 to 21 days). The number of cells existing in the surface region is N_s, and that in the inner region is N_i. Specimens are ACGS-MS$^-$, ACGS-MS$^+$, ICGS-MS$^-$, and IGCS-MS$^+$. The asterisk symbol (*) indicates a significance of $p < 0.05$.

interface between the concentrated and diluted phases to construct a toroidally aggregating structure, and collect collagen fibrils to the center of the diluted phase (Figure 5C).

In the top layer of ACGS, collagen fibrils would distribute randomly as in ICGS. Significant differences in cell behavior in ACGS from that in ICGS were observed only in the inner regions. In ICGS specimens, the number of the cells inside ICGS seemed to increase with the application of MS. In ACGS specimens, the morphology or orientation of osteoblastic cells in surface regions were almost similar to that of ICGS.

As for the shape of cells in ACGS and ICGS, according to the magnified images, each of the cells in all the images is essentially in the spindle shape, although aggregates of cells look dendritic. However, there are cells in ACGS that appear slightly different from those in ICGS. To understand this difference, information should be needed, after further investigation.

To analyze the invasion ability of osteoblastic cells to matrix quantitatively, we counted the number of the cells distributed in surface and inner regions (Figure 6). The ratio of the number of cells existing in the inner region to the total cell number is expressed as

$$\frac{N_i}{N_i + N_s} \tag{1}$$

where N_i and N_s are the number of cells existing in the inner and surface regions, respectively. In all specimens, almost all cells existed in surface regions and only several cells were found in inner regions after 7 days of cultivation, where the number of cells was larger for ACGS than ICGS. After 14 days of cultivation, significant increases in cells remaining in the inner regions were observed in all specimens. Approximately 30% of cells invaded into the inner regions in ACGS, while only 20% of cells existed in the inner regions in ICGS. In 21-day culture specimens, however, no significant increases in cell numbers in the inner regions were observed in all specimens. Cell invasion seems to have been saturated after 14 days. In ICGS specimens, MS seems to promote the significant invasion of osteoblastic cells to the matrix after days 7 and 14, as in other reports.[29−31] However, such a change by MS was not observed in ACGS specimens. These results indicate that the MS effect on the invasion ability of osteoblastic cells is much smaller than that of the ACGS anisotropic structure.

2. Small Angle X-ray Scattering. Two-dimensional (2D) small-angle X-ray scattering (SAXS) patterns for ACGS, ICGS, ACGS-MS$^-$, ACGS-MS$^+$, ICGS-MS$^-$, and ICGS-MS$^+$ are shown in Figure 4 in the Supporting Information.

2.1. Scattering from ACGS and ICGS. Log−log plots of SAXS profiles for ACGS and the ICGS are shown in Figure 7A. At the low-q region ($0.02\ \text{nm}^{-1} < q < 0.04\ \text{nm}^{-1}$), the logarithm of $I(q)$ for ACGS linearly decreased with an increasing logarithm of q. At the high-q region ($q > 0.04\ \text{nm}^{-1}$), logarithms of $I(q)$ for ACGS also decreased linearly as the logarithm of q increased, but with a steeper slope. Therefore, SAXS profiles $I(q)$ for ACGS can be regarded to consist of two power-law regions, a low-q region and a high-q region. The power law relationship between $I(q)$ and q can be expressed as

$$I(q) \propto q^{-a} \tag{2}$$

where a is the scattering exponent of the power-law. Scattering exponents were calculated from the slopes of linear regions in the log−log plot. The scattering exponent at the low-q region, $a_{\text{low-}q}$, for ACGS ($a_{\text{low-}q} = 2.07 \pm 0.04$) was smaller than that at the high-q region, $a_{\text{high-}q}$, for ACGS ($a_{\text{high-}q} = 3.53 \pm 0.11$). Scattering exponents have been reported to be related to the fractal dimensions of the structure of scattering bodies.[32] The $a_{\text{low-}q}$ is attributed to a mass fractal dimension (D_m). The mass fractal dimension has a value of 1−3 and is related to the compactness of the scattering bodies packing. The relationship between the $a_{\text{low-}q}$ and D_m is expressed as

$$D_m = a_{\text{low-}q} \tag{3}$$

Small values of D_m indicate looser structures and large values of D_m indicate compact structures. On the other hand, $a_{\text{high-}q}$ is related to a surface fractal dimension (D_s). The surface fractal dimension has a value of 2−3 and relates to the roughness of the surface of the scattering bodies. The relationship between $a_{\text{high-}q}$ and D_s is expressed as

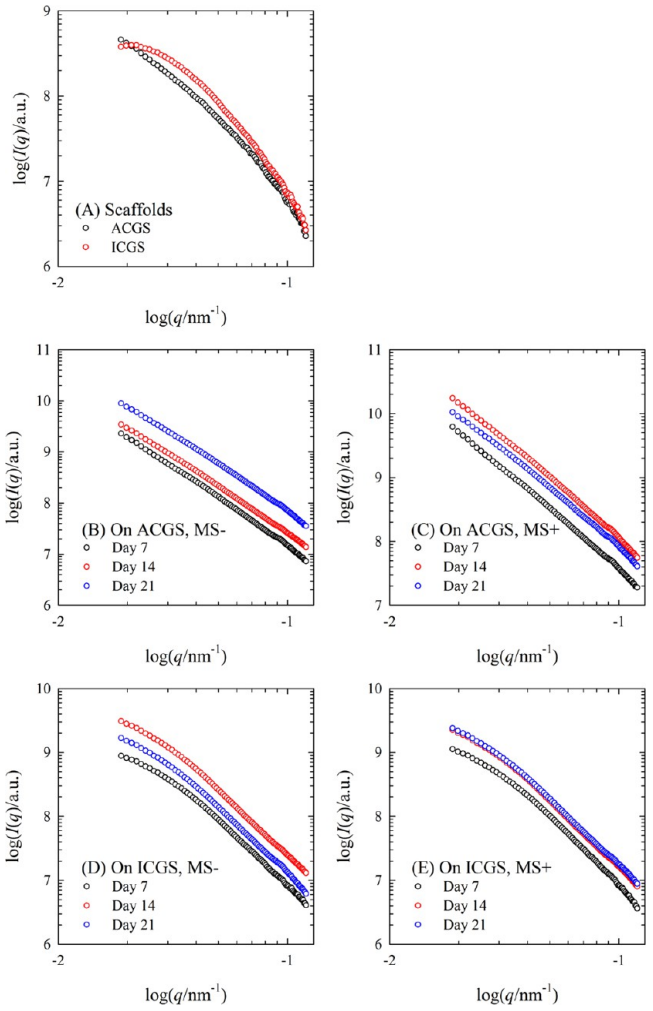

Figure 7. Log–log plots of SAXS profiles for scaffolds (A) and cell-seeded specimens (B–E). Specimens are: (A) ACGS and ICGS, (B) ACGS-MS$^-$, (C) ACGS-MS$^+$, (D) ICGS-MS$^-$, and (E) ICGS-MS$^+$. Cell-seeded specimens were cultured for 7, 14, and 21 days.

$$D_s = 2D - a_{\text{high-}q} \quad (4)$$

where D is the dimension of the scattering bodies. For 3D scattering bodies, $D = 3$. If D_s is small, the surface of the scattering bodies is smooth. On the other hand, if D_s is large, the surface of the scattering bodies is rough.

No linear region was observed at the low-q region in the log–log plot for ICGS. On the other hand, the logarithm of $I(q)$ at the high-q region in the log–log plot for ICGS linearly decreased as the logarithm of q increased. There was no significant difference between the $a_{\text{high-}q}$ values for ACGS and for ICGS.

Consequently, in the low-q region, the linear region was observed only in ACGS. However, in the high-q region, the linear relation in $I(q)$ vs q was observed in both ACGS and ICGS. There was no significant difference between $a_{\text{high-}q}$ values for ACGS and for ICGS.

2.2. Scattering from Cell-Seeded ACGS. Log–log plots of SAXS profiles for cell-seeded scaffolds are shown in Figures 7B–E. In all specimens, the scattering intensity was increased by cell seeding, although the increment did not change in the order of the culturing period. During cell culturing, decrease in the volume of the scaffold was observed, resulting in an increase in the concentration of collagen fibrils in the scaffolds. The increase in scattering intensity can be attributed to these changes in the scaffolds. A weak scattering maximum was observed near q_m = 0.093 nm^{-1} in all specimens. Spacing corresponding to the q_m value calculated from Bragg's law was 67.5 nm. Since the value was almost equal to the D-period of collagen fibrils, results suggest that the scattering behavior is mainly due to collagen fibrils and/or aggregates of collagen fibrils.

To discuss changes in the higher-order structure of collagen fibrils in cell-seeded specimens, scattering behavior in the q range from 0.018 nm^{-1} to q_m were further analyzed. Scattering curves from ACGS-MS$^-$ and ACGS-MS$^+$ have two power-law regions: the low-q region (0.018 nm^{-1} < q < 0.04 nm^{-1}) and high-q region (0.04 nm^{-1} < q < 0.08 nm^{-1}) (see Figures 7B and 7C). We calculated $a_{\text{low-}q}$ and $a_{\text{high-}q}$ from the slope of the straight lines in log–log plots for ACGS-MS$^-$ and ACGS-MS$^+$. Changes in $a_{\text{low-}q}$ and $a_{\text{high-}q}$, along with the cultivation times, are shown in Figures 8A and 8B. At day 7, values of $a_{\text{low-}q}$ for ACGS increased from 2.07 ± 0.04 to 2.95 ± 0.02 for ACGS-MS$^-$ and to 3.02 ± 0.03 for ACGS-MS$^+$ by cell seeding. After day 7, $a_{\text{low-}q}$ decreased as the cultivation time increased. Values of $a_{\text{low-}q}$ were in the range of 1–3, indicating the mass fractal dimension. The increase in $a_{\text{low-}q}$ due to cell seeding indicates that scattering

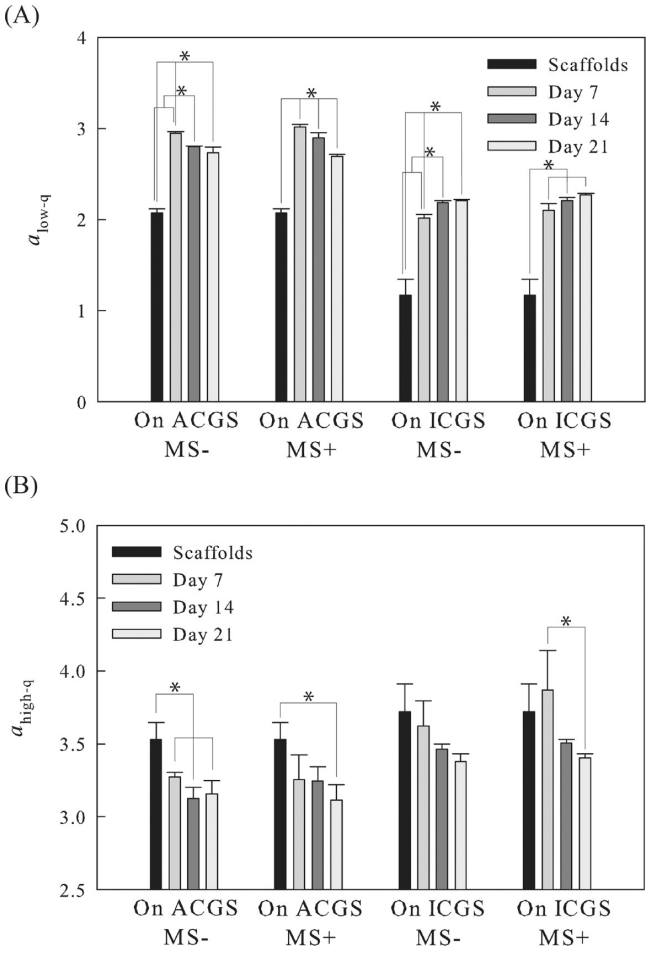

Figure 8. Scattering exponents determined from slopes of the straight lines in (A) the low-q region and (B) the high-q region in log–log plots of SAXS profiles. Specimens are ACGS, ICGS, ACGS-MS$^-$, ACGS-MS$^+$, ICGS-MS$^-$, and ICGS-MS$^+$. Cell-seeded specimens were cultured for 7, 14, and 21 days. The asterisk symbol (*) indicates a significance of p < 0.05.

bodies are packed more compactly. The decrease in $a_{low\text{-}q}$ after day 7 of culture suggests that the packing of the scattering bodies becomes loose as the cultivation time increases. There were no significant changes in the values of $a_{high\text{-}q}$ during cell culturing, irrespective of cultivation conditions (Figure 8B). Since the values of $a_{high\text{-}q}$ were in the range of 3−4, the values of $a_{high\text{-}q}$ are related to the surface fractal dimension. This result demonstrates that the roughness of the bodies in ACGS-MS$^-$ and ACGS-MS$^+$ does not change during the cell culture. No significant effects of mechanical stress on changes in both $a_{low\text{-}q}$ and $a_{high\text{-}q}$ were observed.

2.3. Scattering from Cell-Seeded ICGS. For both ICGS-MS$^-$ and ICGS-MS$^+$, two linear regions were observed at the low-q region ($0.018\ nm^{-1} < q < 0.03\ nm^{-1}$) and the high-$q$ region ($0.05\ nm^{-1} < q < 0.08\ nm^{-1}$) in log−log plots, respectively (see Figures 7D and 7E). Values of $a_{low\text{-}q}$ for ICGS-MS$^-$ and ICGS-MS$^+$ increased as the cultivation time increased. Values of $a_{low\text{-}q}$ for ICGS-MS$^-$ and ICGS-MS$^+$ were in the range of 1−3, indicating the mass fractal dimension. Therefore, the increase in the $a_{low\text{-}q}$ for ICGS-MS$^-$ and ICGS-MS$^+$ suggests that the packing of the scattering bodies becomes tight with the cell culture. There were no significant changes in the values of $a_{high\text{-}q}$ during the cell culture, regardless of the cultivation conditions (see Figure 8B). Since the values of $a_{high\text{-}q}$ were in the range of 3−4, the values are related to the surface fractal dimension. This result indicates that the roughness of the surface of scattering bodies in ICGS-MS$^-$ and ICGS-MS$^+$ does not change during the cell culture. No significant effects of mechanical stress on changes in the $a_{low\text{-}q}$ were observed.

2.4. Size of Scattering Bodies. To determine characteristic sizes of scattering bodies in specimens, the scattering intensity in the q range between $0.018\ nm^{-1}$ and $0.08\ nm^{-1}$ was analyzed by the modified Guinier analysis.[33] The collagen fibril can be regarded as a rodlike particle with contour length L, cross-sectional area A, and cross-sectional radius R_c. For the q-range between $1/L$ and $1/r_c$, the scattering intensity of the rodlike particle is approximately expressed as

$$I(q) \approx \frac{\pi A^2 \Delta\rho}{qL} e^{-r_c^2 q^2/2} \quad (5)$$

where $\Delta\rho$ is the difference in electron density between that of rodlike particles and solvent, and r_c is the radius of the gyration of the cross-section of rodlike particles. For the circular cross-section, $r_c = R_c/\sqrt{2}$. The values of r_c were calculated from the slopes of the straight lines in cross-sectional Guinier plots ($\ln qI(q)$ vs q^2). Cross-section Guinier plots for ACGS and ICGS are shown in Figure 9A. Two linear regions are observed in cross-section Guinier plots for both scaffolds. Shapes of cross-sectional Guinier plots suggest the polydispersity of r_c of the rodlike particles. Therefore, ACGS and ICGS consisted of rodlike particles with various diameters. From an initial slope of the cross-section Guinier plot, we calculated a radius of the cross-section for thick rodlike particles ($R_{c,l}$). On the other hand, a cross-sectional radius of the thin rodlike particles ($R_{c,s}$) was calculated from the slope of the linear region observed in the high-q region of the cross-sectional Guinier plot. The $R_{c,l}$ for ACGS was larger than that for ICGS, whereas $R_{c,s}$ for ACGS was approximately equal to that for ICGS, as shown in Figures 10A and 10B, respectively. The $R_{c,s}$ value of ~60 nm for ACGS and ICGS was almost equal to the radius of a single collagen fibril reported in the literature.[34] Thus, $R_{c,s}$ would be the radius of a single collagen fibril. On the other hand, in the literature, it

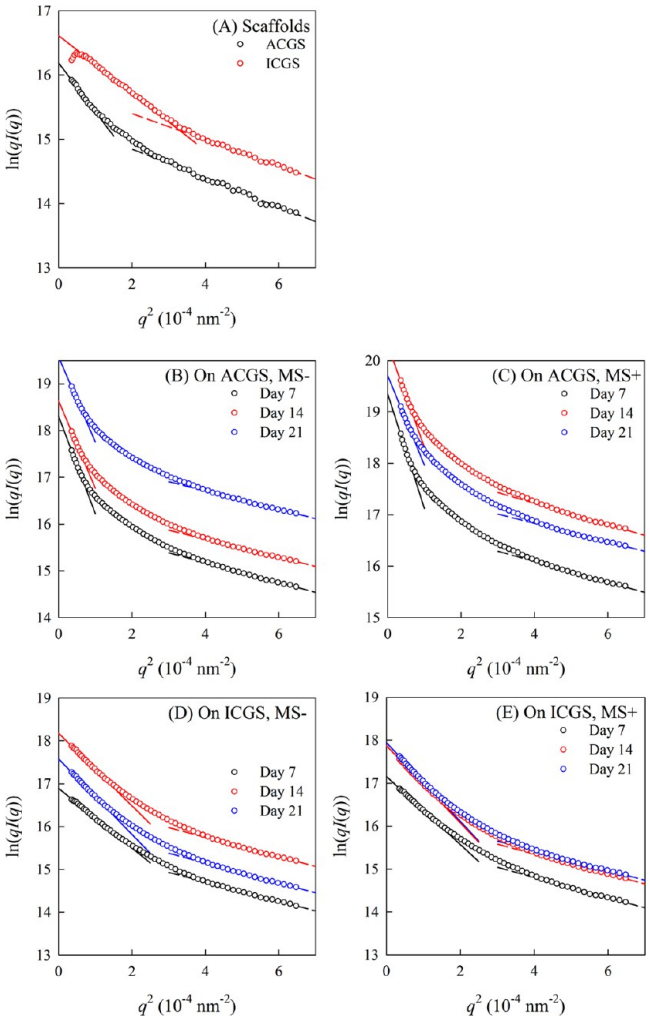

Figure 9. Cross-sectional Guinier plots of SAXS profiles for (A) scaffolds and (B−E) cell-seeded specimens. Specimens are: (A) ACGS and ICGS, (B) ACGS-MS$^-$, (C) ACGS-MS$^+$, (D) ICGS-MS$^-$, and (E) ICGS-MS$^+$. Cell-seeded specimens were cultured for 7, 14, and 21 days.

was also reported that bundles of collagen fibrils were formed in the collagen hydrogel prepared from the acid-soluble collagen.[35] The $R_{c,l}$ for ACGS and ICGS were comparable with radii of the bundles of collagen fibrils reported in the literature. Therefore, the $R_{c,l}$ could correspond to the radius of the bundles of collagen fibrils.

$R_{c,l}$ for ACGS-MS$^-$ and ACGS-MS$^+$ increased with cell seeding, and then decreased as the culture time increased. On the other hand, $R_{c,l}$ for ICGS-MS$^-$ and ICGS-MS$^+$ increased with cell seeding, and then increased with increases in the culture time. In all specimens, no significant changes in $R_{c,s}$ were observed. The results suggest that the remodeling process of bundles of collagen fibrils is dependent on the scaffold structure, whereas that of the collagen fibril itself is independent of the scaffold structure. No significant effect of the mechanical force on changes in $R_{c,l}$ and $R_{c,s}$ was observed.

3. Relationship between Macroscopic and Microscopic Observations in ACGS. In the macroscopic observation, collagen fibrils were modified by osteoblastic cells in ACGS (Figure 4E). In the microscopic observation, the packing and bundle diameter of collagen fibrils were changed both in ACGS and ICGS (see Figures 8 and 10), and

dx.doi.org/10.1021/am303254e | ACS Appl. Mater. Interfaces 2013, 5, 5937−5946

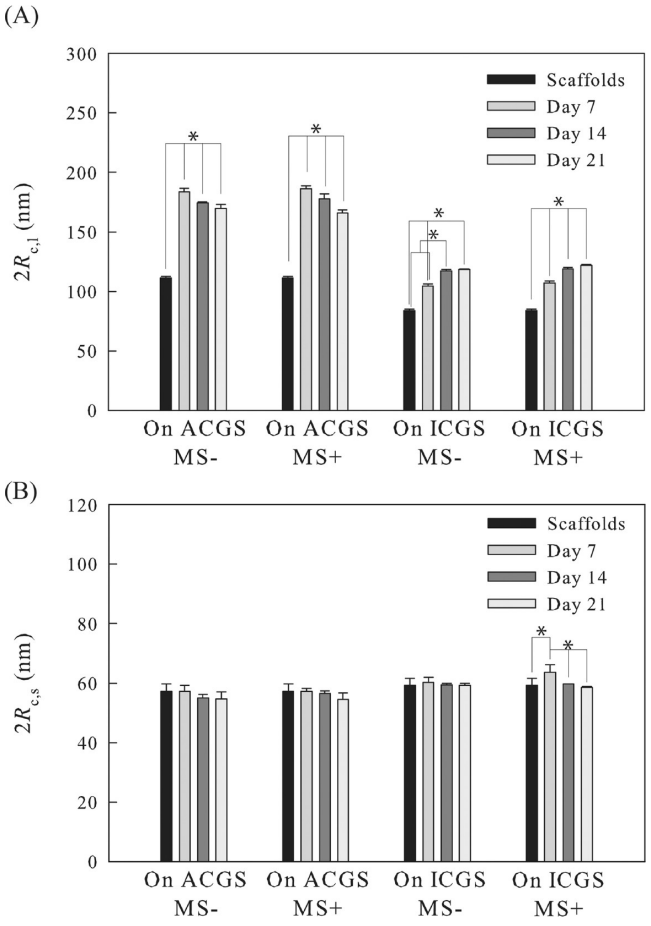

Figure 10. Diameters of (A) the bundles of collagen fibrils and (B) a single collagen fibril determined by the modified Guinier analysis. Specimens are ACGS, ICGS, ACGS-MS$^-$, ACGS-MS$^+$, ICGS-MS−, and ICGS-MS$^+$. Cell-seeded specimens were cultured for 7, 14, and 21 days. $R_{c,l}$ was estimated by the cross-sectional radius of the thick rodlike particles. $R_{c,s}$ was the cross-sectional radius for thin rodlike particles, which was determined from the slope of the linear region observed in the high-q region of the cross-sectional Guinier plot.

remodeling process of the collagen bundles in ACGS was different from that in ICGS (Figure 10). These results indicate that the bundles of collagen fibrils are reconstructed by osteoblastic cells. In this experimental system, there would be two species of collagen molecules: (1) matrix collagen molecules originated from bovine atelo-collagen, and (2) osteoblastic cell-secreted collagen molecules. As mentioned above, the diameter of collagen fibrils was reported to be ∼50 nm.[34] The diameter of collagen fibers produced by osteoblasts was reported to be 30−45 nm in 8−12 days of culture.[36] Therefore, we cannot determine the origin of the collagen fibrils obtained here from the diameter. The diameter of collagen fibrils was changed after seeding of osteoblastic cells; thus, collagen fibrils appear to be modified by osteoblastic cells. Collagen fibrils were collected in the diluted phase in ACGS. These collagen fibrils seemed to be the matrix collagen, because osteoblasts may not produce such thick fibrils.

These results suggest that osteoblastic cells change the diameter of collagen fibrils and both cell- and matrix-derived collagen fibrils are modified by the cells both in ACGS and ICGS. Remodeling of collagen fibrils would be affected by the difference of the scaffold structure.

4. Mechanical Stimulation (MS) for Osteoblastic Behaviors. Mechanical stimulation (MS) has long been revealed as being crucial for osteogenesis. Osteogenesis can be regarded as one of phenotypes of osteoblastic cells-ECM interaction. In our results on MC3T3-E1 osteoblastic cell and ECM interaction, however, the effect of MS was not clearly observed in ACGS specimens, while MS significantly increased the invasion of osteoblastic cells into the ICGS matrix. One explanation for the ineffectiveness of MS on the osteogenensis in our case could be this: (1) the MS applied here was not optimum. The strain and frequency of the applied MS are 3000 $\mu\varepsilon$ and 3 Hz, these parameters mimic MS exposed to bone in vivo.[15] Many studies also have applied such high-strain and low frequency MS for osteoblastic cells.[20−22,24] Contrary to this, there are reports that conditions of low strain and high frequency are more effective for osteoblastic differentiaion in previous reports.[37,38] Furthermore, Dumas et al. used the combinations of high strain and low frequency and low strain and high frequency; this dual-frequency cyclic strain was enhanced by osteoblast differentiation.[39] Another possibility is a period and timing of MS application. Some responses to MS, such as an increase in the amount of intracellular Ca^{2+}, is a fast process; MS effects diminish just after MS application. However, Kreke et al. reported that the osteoblastic gene was up-regulated 13 days after the application of MS was stopped.[40]Optimization of the application of MS would be needed to enhance the matrix remodeling activity of osteoblastic cells. Another explanation would be this: (2) Changes in ECM by MS are located far downstream the events of immediate response to MS such as gene or protein expressions. There is a possibility that the change in ECM would not be detected, even though gene or protein expressions were observed.

However, both of these do not present a convincing explanation for the selective effect of MS on ICGS. The plausible explanation for our results may be that the MS applied in the experiments was not an optimum one for ACGS, although the MS parameters have been said to be normal in an animal's life. However, it is also a fact that the MS that is applied to a scaffold is not necessarily optimum to scaffolds having different structures and mechanical properties; further biological study is needed to fully understand the effect of MS application on osteoblastic behavior, although it is beyond the scope of the present study.

5. Effect of Diluted Phase Diameter in ACGS for Osteoblast Behavior. In ACGS samples, osteoblastic cells in the shallow region of the scaffold exhibited different behavior from that in the deep region. In the shallow region, the cells collected the collagen fibrils in the diluted phase (Figure 5B). However, in the deep region, the cells would attach on the interface between concentrated and diluted phases to construct a toroidally aggregating structure, and they collected collagen fibrils at the center of the diluted phase (Figure 5C). Furthermore, the cells attached only on the interface in deeper regions of the diluted phase (data not shown). However, osteoblastic cells uniformly existed in the inner region of ICGS, and such a scaffold-structure-dependent cell behavior was not observed in ICGS (see Figures 4A and 4B). The results suggest that the morphology of the osteoblastic cell would be changed with the diameter of diluted phase. Therefore, if we can control the diameter of the diluted phase, cell behavior in the diluted phase could be controlled. In fact, the diameter or number of diluted phases can be easily and broadly controlled by changing

the temperature, ionic strength, pH, and collagen concentration.[41] Figures 6(A)−(E) in the Supporting Information indicate that we can control the diameter of the diluted phase by changing the gelling temperature. These controllable features of ACGS indicate a high potential ability as a novel scaffold material in tissue engineering.

6. Application of Scaffold for Osteoblastic Cell Cultivation. In this experiment, we focused on the matrix remodeling function of osteoblastic cells. We performed calcium deposition analysis on another anisotropic gel scaffold to confirm the osteoinductive potential of ACGS (see Figure 5 in the Supporting Information). The results showed that anisotropic gel structure enhanced hydroxyapatite deposition of osteoblastic cells and confirmed ability as a scaffold for expected osteogenesis. Therefore, ACGS is a suitable scaffold for bone-mimicking material.

CONCLUSION

By culturing osteoblastic cells on an anisotropic collagen gel scaffold (ACGS), the interaction of cells with the scaffold was investigated focusing on how the scaffold structure was remodeled from molecular rearrangements to macroscopic morphology. As has been expected, cells favored staying in pliant dilute phase in ACGS. The dilute phase is in a tapered cylinder shape along the thickness direction, where the diameter of the dilute phase increased with the depth from the surface. Immediately below the surface of ACGS, where the size of the diluted phase is comparable to that of cells, a cell placed at the center of the phase and appeared to be interwoven with collagen fibers. In the deep region, cells attached onto the interface between the diluted and the concentrated phases and aggregated in a toroidal shape. Through the interaction with cells, local packing state of collagen fibers in ACGS was changed. Along with the gradual change in the gel structure, the interaction of cells with the scaffold also changed. We consider the cell function of scaffold contracting force generation after anchoring on the matrix would underlie the phenomena observed. Since it is possible to control the structure of ACGS by regulating the temperature, ionic strength, pH, and collagen concentration during preparation,[41] the cells−scaffold interaction can be also controllable, which may promise tailor-made tissue engineering.

ASSOCIATED CONTENT

Supporting Information

Macroscopic morphology of ACGS and ICGS, schema of applied strain amplitude to cell-gel composites and of X-ray beam radiation geometry to a specimen, 2D SAXS patterns of scaffolds and cell-seeded specimens, Wide-angle X-ray diffraction (WAXD) analysis of the anisotropic and isotropic collagen gel with osteoblastic cell cultivation, example for morphological regulation of ACGS were presented in Supporting Information. It is available free of charge via the Internet at http://pubs.acs.org.

AUTHOR INFORMATION

Corresponding Author

*Fax: +81-11-706-2569. E-mail: nasa5131@sci.hokudai.ac.jp.

Notes

The authors declare no competing financial interest.

ACKNOWLEDGMENTS

N.S gratefully acknowledges support from the Grant-in-Aid for Scientific Research (C) (No. 21500401) from JSPS, and K.F. appreciates support from Akiyama Life Science Foundation. Synchrotron radiation experiments were performed at the BL40B2 of SPring-8 with the approval on the Japan Synchrotron Radiation Research Institute (JASRI) (Proposal No. 2011B1667).

REFERENCES

(1) Kunz-Schughart, L. A.; Wenninger, S.; Neumeier, T.; Seidl, P.; Knuechel, R. *Am. J. Physiol. Cell Physiol.* **2003**, *284*, 209−219.
(2) Kleinman, H. K.; Philp, D.; Hoffman, M. P. *Curr. Opin. Biotechnol.* **2003**, *14*, 526−532.
(3) Chen, S. S.; Falcovitz, Y. H.; Schneiderman, R.; Maroudas, A.; Sah, R. L. *Osteoarthritis Cartilage* **2001**, *9* (6), 561−569.
(4) Jung, T.-K.; Matsumoto, H.; Abumiya, T.; Masahashi, N.; Kim, M.-S.; Hanada, S. *Mater. Sci. Forum* **2010**, *631*−*632*, 205−210.
(5) Lanfer, B.; Seib, F. P.; Freudenberg, U.; Stamov, D.; Bley, T.; Bornhäuser, M.; Werner, C. *Biomaterials* **2009**, *30*, 5950−5958.
(6) Lai, E. S.; Anderson, C. M.; Fuller, G. G. *Acta Biomater.* **2011**, *7*, 2448−2456.
(7) Isobe, Y.; Kosaka, T.; Kuwahara, G.; Mikami, H.; Saku, T.; Kodama, S. *Materials* **2012**, *5*, 501−511.
(8) Mikami, H.; Kuwahara, G.; Nakamura, N.; Yamato, M.; Tanaka, M.; Kodama, S. *J. Urol.* **2012**, *187*, 1882−1889.
(9) Caliari, S. R.; Weisgerber, D. W.; Ramirez, M. A; Kelkhoff, D. O.; Harley, B. A. C. *J. Mech. Behav. Biomed. Mater.* **2012**, *11*, 27−40.
(10) Guido, S.; Tranquillo, R. T. *J. Cell Sci.* **1993**, *105*, 317−331.
(11) Furusawa, K.; Sato, S.; Masumoto, J.; Hanazaki, Y.; Maki, Y.; Dobashi, T.; Yamamoto, T.; Fukui, A.; Sasaki, N. *Biomacromolecules* **2012**, *13*, 29−39.
(12) Furusawa, K.; Sato, S.; Masumoto, J.; Hanazaki, Y.; Maki, Y.; Dobashi, T.; Yamamoto, T.; Fukui, A.; Sasaki, N. *Biomacromolecules* **2012**, *13*, 1232−1232.
(13) Tang, S. Y.; Herber, R.-P.; Ho, S. P.; Alliston, T. *J. Bone Miner. Res.* **2012**, *27*, 1936−1950.
(14) Robling, A. G.; Castillo, A. B.; Turner, C. H. *Annu. Rev. Biomed. Eng.* **2006**, *8*, 455−498.
(15) Duncan, R. L.; Turner, C. H. *Calcif. Tissue Int.* **1995**, *57*, 344−358.
(16) Rubin, J.; Rubin, C.; Jacobs, C. R. *Gene* **2006**, *367*, 1−16.
(17) Kapur, S.; Baylink, D. J.; Lau, K. H. *Bone* **2003**, *32*, 241−251.
(18) Datta, N.; Pham, Q. P.; Sharma, U.; Sikavitsas, V. I.; Jansen, J. A.; Mikos, A. G. *Proc. Natl. Acad. Sci. U.S.A.* **2006**, *103*, 2488−2493.
(19) Bancroft, G. N.; Sikavitsas, V. I.; van den Dolder, J.; Sheffield, T. L.; Ambrose, C. G.; Jansen, J. A.; Mikos, A. G. *Proc. Natl. Acad. Sci. U.S.A.* **2002**, *99*, 12600−12605.
(20) Walker, L. M.; Publicover, S. J.; Preston, M. R.; Said Ahmed, M. A.; El Haj, A. J. *J. Cell. Biochem.* **2000**, *79*, 648−661.
(21) Liu, J.; Liu, T.; Zheng, Y.; Zhao, Z.; Liu, Y.; Cheng, H.; Luo, S.; Chen, Y. *Biochem. Biophys. Res. Commun.* **2006**, *348*, 1167−1173.
(22) Rath, B.; Nam, J.; Knobloch, T. J.; Lannutti, J. J.; Agarwal, S. *J. Biomech.* **2008**, *41*, 1095−1103.
(23) Ziros, P. G.; Gil, A. P.; Georgakopoulos, T.; Habeos, I.; Kletsas, D.; Basdra, E. K.; Papavassiliou, A. G. *J. Biol. Chem.* **2002**, *277*, 23934−23941.
(24) Guo, Y.; Zhang, C.; Zeng, Q.; Li, R.; Liu, L.; Hao, Q.; Shi, C.; Zhang, X.; Yan, Y. *Biomed. Eng. Online* **2012**, *11*, 80.
(25) Li, Y.; Ge, C.; Long, J. P.; Begun, D. L.; Rodriguez, J. A; Goldstein, S. A.; Franceschi, R. T. *J. Bone Miner. Res.* **2012**, *27*, 1263−1274.
(26) Engler, A. J.; Sen, S.; Sweeney, H. L.; Discher, D. E. *Cell* **2006**, *126*, 677−689.
(27) Guilak, F.; Cohen, D. M.; Estes, B. T.; Gimble, J. M.; Liedtke, W.; Chen, C. S. *Cell Stem Cell* **2009**, *5*, 17−26.
(28) Reilly, G. C.; Engler, A. J. *J. Biomech.* **2010**, *43*, 55−62.
(29) Davis, G. E.; Senger, D. R. *Circ. Res.* **2005**, *97*, 1093−1107.

(30) Shieh, A. C.; Rozansky, H. A.; Hinz, B.; Swartz, M. A. *Cancer Res.* **2011**, *71*, 790−800.
(31) Menon, S.; Beningo, K. A. *PLoSOne* **2011**, *6*, e17277.
(32) Martin, J. E.; Hurd, A. J. *J. Appl. Crystallogr.* **1987**, *20*, 61−78.
(33) Glatter, O.; Kratky, O. *Small Angle X-ray Scattering*; Academic Press: London, 1982; pp 32−35.
(34) Wood, G. C.; Keech, M. K. *Biochem. J.* **1960**, *75*, 588−598.
(35) Raub, C. B.; Suresh, V.; Krasieva, T.; Lyubovitsky, J.; Mih, J. D.; Putnam, A. J.; Tromberg, B. J.; George, S. C. *Biophys. J.* **2007**, *92*, 2212−2222.
(36) Garstenfeld, L. C.; Riva, A.; Hodgens, K.; Eyre, D. R.; Landis, W. J. *J. Bone Miner. Res.* **1993**, *8*, 1031−1043.
(37) Patel, M. J.; Chang, K. H.; Sykes, M. C.; Talish, R.; Rubin, C.; Jo, H. *J. Cell. Biochem.* **2009**, *106*, 306−316.
(38) Dumas, V.; Ducharne, B.; Perrier, A.; Fournier, C.; Guignandon, A.; Thomas, M.; Peyroche, S.; Guyomar, D.; Vico, L.; Rattner, A. *Calcif. Tissue Int.* **2010**, *87*, 351−364.
(39) Dumas, V.; Perrier, A.; Malaval, L.; Laroche, N.; Guignandon, A.; Vico, L.; Rattner, A. *Biomaterials* **2009**, *30*, 3279−3288.
(40) Kreke, M. R.; Sharp, L. A.; Lee, Y. W.; Goldstein, A. S. *Tissue Eng., Part A* **2008**, *14*, 529−537.
(41) Furusawa, K. Private communication.